Computer Modelling and New Technologies, 2010, Vol.14, No.2, 7–19
Transport and Telecommunication Institute, Lomonosova 1, LV-1019, Riga, Latvia

THEORETICAL RESISTANCE SIMULATIONS FOR JUNCTIONS OF SW AND MW CARBON NANOTUBES WITH METAL SUBSTRATES IN NANOELECTRONIC DEVICES

Yu. N. Shunin[1,2], Yu. F. Zhukovskii[2], N. Burlutskaya[1], V. I. Gopeyenko[1], S. Bellucci[3]

[1]Information Systems Management Institute, Riga, Latvia
[2]Institute of Solid State Physics, University of Latvia, Riga, Latvia
[3]INFN-Laboratori Nazionali di Frascati, Via Enrico Fermi 40, Frascati, Italy
E-mails : shunin@isma.lv[1,2], quantzh@latnet.lv[2], natalja.burlucka@isma.lv[1], Viktors.Gopejenko@isma.lv[1], Stefano.Bellucci@lnf.infn.it[3]

In the current study, basic attention is paid to the junctions of carbon nanotubes (CNTs) with contacting metallic elements of a nanocircuit. Numerical simulations on the conductance and resistance of these contacts have been performed using the multiple scattering theory and the effective media cluster approach. Two models for CNT-metal contacts have been considered in this paper: a) first principles "liquid metal" model and b) empirical model of "effective bonds" based on Landauer notions on ballistic conductivity. Within the latter we have simulated both single-wall (SW) and multi-wall (MW) CNTs with different morphology. Results of calculations on resistance for different CNT-Me contacts look quantitatively realistic (from several to hundreds kOhm, depending on chirality, diameter and thickness of MW CNT). The inter-wall transparency coefficient for MW CNT has been also simulated, as an indicator of possible 'radial current' losses.

Keywords: *carbon nanotubes, single-wall and multi-wall morphology, nanotube-metal (CNT-Me) junction, scattering theory, electronic structure calculations, conductance and resistance in CNT-Me contact, inter-wall transparency in CNTs*

1. Introduction

The miniaturization of electronic devices, the high integration level and increase of the operation frequencies and power density require the use of adequate materials and innovative chip interconnects and vias, to avoid a bottleneck in the existing technologies. Fundamental efforts are directed on the special kinds of nanosystems such as quantum dots, quantum nanowires and nanotubes. Quantum dots, also known as nanocrystals, are a non-traditional type of semiconductor with limitless applications as an enabling material across many industries. They are unique class of semiconductor, because they are so small, ranging from 2–10 nm. (10–50 atoms) in diameter (Fig. 1). Basic attention is paid to carbon nanotubes (CNTs), including their contacts with other conducting elements of a nanocircuit. Due to the unique physical properties, CNTs attract permanently growing technological interest, for example as promising candidates for nanointerconnects in a future high-speed electronics (Figs. 2, 3).

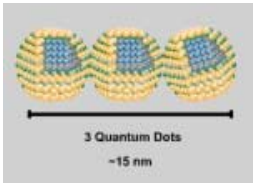

Figure 1. Quantum dots

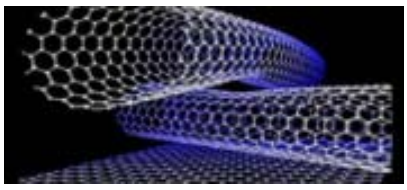

Figure 2. Carbon nanotubes

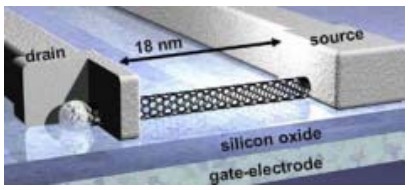

Figure 3. Model of nanoelectronic device

Discovered in 1991 by Iijima and coworkers, carbon nanotubes have quickly become one of the most popular materials in nanoscience and nanotechnology, drawing the interest of researchers worldwide. Many potential applications have been investigated, largely based on theoretical and experimental results, including: conductive and high-strength composites; energy storage and energy conversion devices; sensors; field emission displays and radiation sources; nanometer-sized semiconductor devices, probes, and interconnects.

Due to their unique physical properties, carbon nanotubes (CNTs) attract permanently growing technological interest, for example, as promising candidates for nano-interconnects in a high-speed

electronics [1]. The main aim of the current study is the implementation of advanced simulation models, for a proper description of the electrical resistance for contacts between carbon nanotubes of different morphologies and metallic substrates of different nature.

The resistance of contacts between CNTs and metallic catalytic substrates can considerably exceed that observed in the separate parts of these junctions [2, 3]. The conductance between real metals and CNTs still occurs, however, mainly due to the scattering processes, which are estimated to be rather weak [4]. Figure 4 represents the contacts between a CNT and both substrates, as a prototype nanodevice. This is a main subject of our current research and modelling.

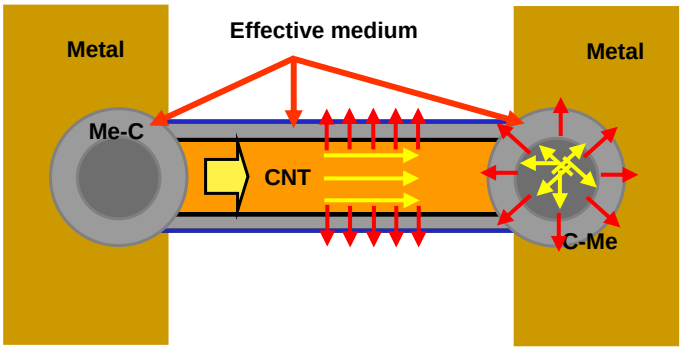

Figure 4. Model of CNT-Me interconnect as a prototype of nanodevice

The toroidal region (CNT-Me) is the object of a microscopic approach responsible for the main contribution to the resistance. As to the nanotube itself and the metallic substrate, their resistances may be considered as macroscopic parameters.

The electronic structure for the CNT-Me interconnect can be evaluated through the electronic density of states (DOS) for carbon-metal contact considered as a 'disordered alloy', where clusters containing both C and Me atoms behave as scattering centers. The computational procedure developed by us for these calculations [5] is based on the construction of cluster potentials and the evaluation of both scattering (S) and transfer (T) matrices.

The general model of multiple scattering with effective media approximation (EMA) for condensed matter based on the approach of atomic cluster is presented on Figure 5. The cluster formalism was successfully applied for metallic Cu [5], as well as for both elemental (Ge and Si) and binary (As_xSe_{1-x} and Sb_xSe_{1-x}) semiconductors [6]. A special attention was paid for the latter, since in solid solutions the concept of statistical weighing was applied for the binary components [5, 6]. When using the coherent potential approach (CPA) as EMA approximation, the resistance of interconnect can be evaluated through the Kubo-Greenwood formalism [7] and Ziman model [8]. Both Figures 6 and 7 depict the idealized images of contacts between CNTs and the Ni substrate.

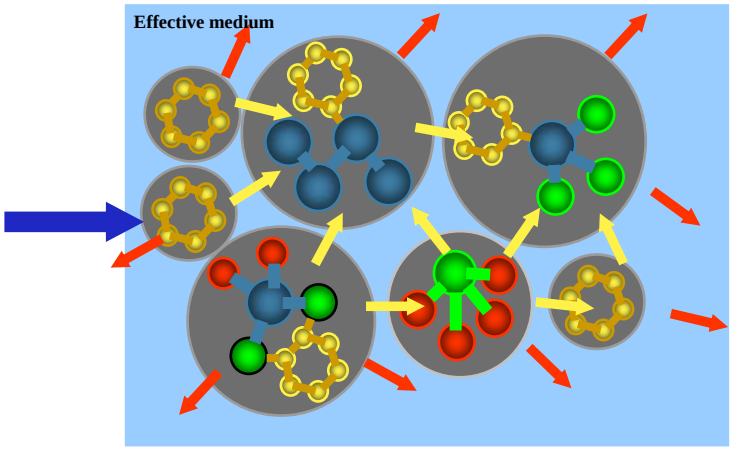

Figure 5. Multiple scattering model of condensed matter described within the effective media approximation

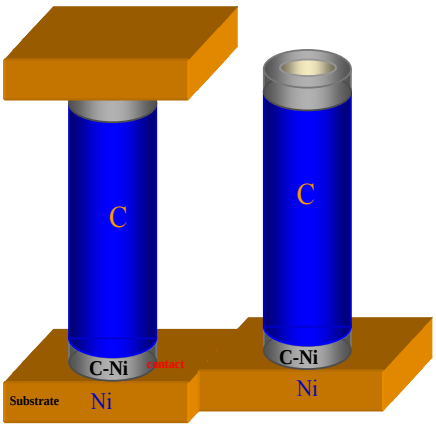

Figure 6. Fragment of interconnects between the Ni substrate and C nanotubes

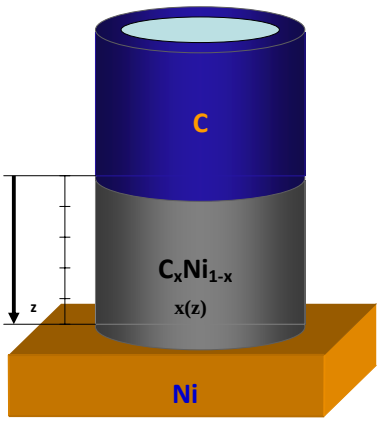

Figure 7. Model of CNT-Ni interconnect as a disordered alloy

The electronic structure for the CNT-Ni interconnects, in the simplest case, can be evaluated through the DOS for C-Ni contact, considered as a 'disordered alloy', where clusters containing carbon and nickel atoms are the scattering centers. However, in many cases, we have to develop more complicated structural models for CNT-metal junctions, based on their precise atomistic structures, which take into account the CNT chirality effect. This is also the subject of the current study. When estimating the resistance of a junction between the nanotube and the substrate, the main problem is caused by the influence of the nanotube chirality on the resistance of SW and MW CNT-Me interconnects (Me = Ni, Cu, Ag, Pd, Pt, Au), for a pre-defined CNT geometry.

2. Multiple Scattering Theory and Effective Medium Approach for CNT Simulations

2.1. Electronic Structure Calculations

We consider the resistivity as a scattering problem, where the current carriers participate in the transport, according to various mechanisms based on the presence of scattering centers (phonons, charge defects, structural defects, *etc.*), including a pure elastic way, called ballistic (Matissien rule). The scattering paradigm is presented on Figure 8. This allows us to realize full-scale electronic structure calculations for condensed matter.

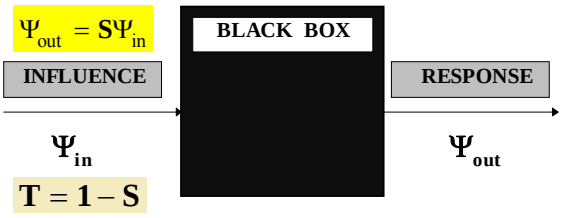

Figure 8. The scattering paradigm: Influence (**in**) and Response (**out**)

We consider a domain where the stationary solutions of the Schrödinger equation are known, and we label them by

$$\psi_{in}(\mathbf{r}) = \phi_{\mathbf{k}}(\mathbf{r}) = exp(i\mathbf{kr}). \tag{1}$$

The scattering of 'trial' waves, in the presence of a potential, yields new stationary solutions labelled by

$$\psi_{out}(\mathbf{r}) = \psi_{\mathbf{k}}^{(\pm)}(\mathbf{r}) \tag{2}$$

for the modified Schrödinger equation $\hat{H}\psi_{\mathbf{k}}^{(\pm)}(\mathbf{r}) = E\psi_{\mathbf{k}}^{(\pm)}(\mathbf{r})$.

An electronic structure calculation is considered here as a scattering problem, where the centers of scattering are identified with the atoms of clusters [5]. The first step in this modeling is the construction

of potentials, both atomic and crystalline, which uses the special well-tested analytical procedures based on the Gaspar-like potentials and X_α- and $X_{\alpha\beta}$- presentations for the electronic exchange and correlation, in the form of electronic density expansions [4] (see, *e.g.,* the carbon potential calculations, Fig. 9).

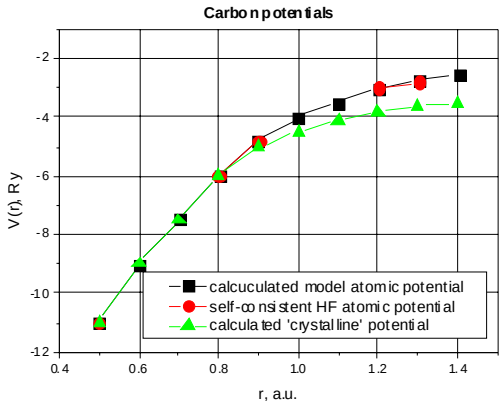

Figure 9. Analytical carbon potentials compared with the results of Hartree-Fock calculations

In order to obtain the electronic structure, the calculations of scattering properties are necessary, generally, in the form of *S*- and *T*-matrices. These calculations start with the definition of the initial atomic structure, to produce a medium for the solution of the scattering problem, for a trial electronic wave [5].

The formalism we use for electronic structure calculations is based on the coherent potential approximation (CPA), the multiple scattering theory and cluster approach. As a *first step* in the modeling procedure, one postulates the atomic structure on the level of short- and medium-range orders. As a *second step* we construct a "crystalline" potential and introduce the muffin-tin (*MT*) approach. This is accomplished by using realistic analytical potential functions.

The scattering paradigm for the simplest cases of spherically symmetrical potential-scatterers (elastic scattering) looks like as follows:

$$\psi(r) \to e^{ikz} + f(\theta)\frac{e^{ikr}}{r} \quad \text{("liquid metal" model case)} \tag{3}$$

and

$$\psi(\mathbf{r}) \to e^{ikz} + f(\theta,\varphi)\frac{e^{ikr}}{r} \quad \text{(spherical cluster model case)} \tag{4}$$

Then, the electronic wave scattering problem is solved, and the energy dependence of the scattering properties for isolated *MT* scatterers is obtained, in the form of the phase shifts $\delta_{lm}(E)$, and the *T*-matrix of the cluster is found as a whole. The indices l and m arise, as a result of expansions of the functions as Bessel's functions j_l, Hankel's functions h_l and spherical harmonics Y_{lm}.

In general, the modelling of disordered materials represents them as a set of atoms or clusters immersed in an effective medium, with the dispersion $E(\mathbf{K})$ and a complex energy-dependent coherent potential $\Sigma(E)$ found self-consistently in the framework of the CPA. The basic equations of this approach are as follows:

$$\Sigma(E) = V_{eff} + \langle T \rangle (1 + G_{eff} \langle T \rangle)^{-1}, \tag{5}$$

$$G(E) = G_{eff} + G_{eff} \langle T \rangle G_{eff} = \langle G \rangle, \tag{6}$$

$$\langle T(E,\mathbf{K}) \rangle = 0, \tag{7}$$

$$\Sigma(E) = V_{eff}, \tag{8}$$

$$\langle G \rangle = G(E) = G_{eff}, \tag{9}$$

$$N(E) = -(2/\pi)\, ln\{det \| G(E) \|\}. \tag{10}$$

Here <...> denotes averaging, V_{eff} and G_{eff} are the potential and the Green's function of the effective medium, respectively, $T(E,\mathbf{K})$ the T matrix of the cluster, and $N(E)$ the integral density of the electronic states. Eq. (5) can be re-written in form:

$$\left\langle T(E,\mathbf{K})\right\rangle = \mathbf{Sp}T(E,\mathbf{K}) = \int_{\Omega_{\mathbf{K}}} \left\langle \mathbf{K}\middle|T(E,\mathbf{K})\middle|\mathbf{K}\right\rangle d\Omega_{\mathbf{K}} = 0, \tag{11}$$

where $\left|\mathbf{K}\right\rangle = 4\pi\sum_{l,m}(\mathrm{i})^{l} j_l(kr)Y^{*}_{lm}(\mathbf{K})Y_{lm}(\mathbf{r})$ is the one-electron wave function and integration is performed over all angles of $\mathbf{K}$ inside the volume $\Omega_{\mathbf{K}}$. Eq. (7) enables one to obtain the dispersion relation $E(\mathbf{K})$ of the effective medium. The DOS calculation in the form of Eq. (10) can be done using the variation principle:

$$\rho(E) = \frac{\delta N(E)}{\delta E}. \tag{12}$$

The paradigm of scattering theory and the developed strategy of simulation of CNTs electronic properties uses the generalized scattering condition for the low-dimensional atomic structures of condensed matter (Quantum Scattering in d-Dimensions):

$$\psi^{(\pm)}_{\mathbf{k}}(\mathbf{r}) \underset{r\to\infty}{\propto} \phi_{\mathbf{k}}(\mathbf{r}) + f^{(\pm)}_{\mathbf{k}}(\Omega)\frac{exp(\pm \mathrm{i}kr)}{r^{\frac{d-1}{2}}}, \tag{13}$$

where superscripts '+' and '–' label the asymptotic behavior in terms of d-dimensional waves:

$$\frac{\partial\sigma_{a\to b}}{\partial\Omega} = \frac{2\pi}{\hbar v}\left|\left\langle \phi_b \middle|\hat{V}\middle|\psi^{+}_{a}\right\rangle\right|^2 \rho_d(E), \tag{14}$$

where d is the atomic structure dimension.

In particular, the scattering model for a cylindrical atomic cluster allows us to calculate below the CNTs electronic structure for various diameters and chiralities.

2.2. Calculations of Conductivity and Resistance

The calculations of conductivity are usually performed using Kubo-Greenwood formula [9]:

$$\sigma_E(\omega) = \frac{\pi\Omega}{4\omega}\int\left[f(E) - f(E+\hbar\omega)\right]\left|D_E\right|^2 \rho(E)\rho(E+\hbar\omega)dE, \tag{15}$$

where ω is a real frequency parameter of Fourier transform for the time-dependent functions, $f(E)$ the Fermi-Dirac distribution function, $D_{E,E'} = \int_{\Omega}\Psi^{*}_{E'}\nabla\Psi_E d\mathbf{r}$, $\Psi_{E(\mathbf{K})} = A\,exp(\mathrm{i}\mathbf{Kr})$ and $\mathbf{K}$ is the complex wave vector of the effective medium. The dispersion function $E(\mathbf{K})$ determines the properties of the wave function $\Psi_{E(\mathbf{K})}$ upon the isoenergy surface in $\mathbf{K}$-space. The imaginary part of $\mathbf{K}$ ($\mathbf{K}_I$) causes a damping of the electron wave, due to the absence of the long-range structural order.

Using the dispersion law, the effective electron mass can be defined as:

$$m^{*} = (\partial^2 E/\partial K_R^2)^{-1}, \tag{16}$$

where K_R is a real part of $K = \|\mathbf{K}\|$. Thus, the static conductivity can be re-written using Drude formula [10]:

$$\sigma_{E(K)} = \frac{e^2 n^{*}}{m^{*}}\tau, \tag{17}$$

where n^* is the effective electron density, with a relaxation time $\tau \approx \frac{l}{v_h}$, $v_h = \left(\frac{3kT}{m^{*}}\right)^{\frac{1}{2}}$, v_h is a heat velocity and l(T) the free path.

Thus, there exist some ideas to estimate the conductivity in static and frequency regimes and take into account temperature effects. However, in the case of CNT, we must consider not only the diffusive mechanism of conductivity, but also the 'so-called' ballistic one. This is an evident complication in the interpretation of electrical properties of CNTs and related systems.

3. 'Liquid Metal' Model for CNT-Metal Junction: *Ni-CNT Case*

The term "liquid" means the structural disorder of the substance involved, more precisely, only the nearest order is taken into account, as it usually occurs in a liquid. It also means that the inter-atomic distance from the nearest neighbour (first coordination sphere) is fixed, whereas the angular coordinates are random. Another condition is that the average density of matter is maintained also locally. A 'liquid metal' model for CNT-Ni junction is based on calculation of the 'mixed' dispersion law [5, 11]:

$$E_{\text{C-Ni}}(\mathbf{K}_{\text{R}}) = xE_{\text{C}}(\mathbf{K}_{\text{R}}) + (1-x)\,E_{\text{Ni}}(\mathbf{K}_{\text{R}}). \tag{18}$$

The metal alloy model is used for evaluation of mixed effective mass $m^*_{\text{C-Ni}}(E)$. Taking into account the spectral dependence of the effective mass $m^*(E)$ and estimating the spectral resistivity $\rho_x(E)$, we should estimate the average layer resistivity $\rho_{x,av}$ as:

$$\rho_{x,av} = \frac{\int_0^{E_{fin}} \rho_x(E)dE}{E_{fin}}, \tag{19}$$

where E_{fin} is the estimated width of conduction band and $x(z)$ the stoichiometry coefficient depending on the coordinate z of ring layer (Fig. 4). An evaluation of resistance for the CNT-Ni contact gives ~ 105 kOhm for the nanotube with the internal and external radii R_1 = 1.0 nm and R_2 = 2.0 nm. Evidently, the results of resistance evaluation for interconnect depend essentially on both the layer height l_0 (C_xNi_{1-x} space, Fig. 7) the spectral integration parameter E_{fin}, which is responsible for the electron transport of really activated electrons. The "liquid metal" model does not take into account CNT chirality in the interconnect space. For this aim, we must construct a model with the realistic atomic structure.

4. Simulation of CNT-Me Interconnect: *'Effective Bonds' Model*

A model of the CNT-Me nanointerconnect [4] (Fig. 4) is developed in the current study. Within the electronic transport formalism, it consists of two regions supporting the two different electron transport mechanisms: ballistic (elastic) and collisional (non-elastic). These electron transport processes are simulated by the corresponding boundary conditions in the form of the effective medium. The CNT chirality (m, n) is simulated by the corresponding orientation of carbon rings within the scattering medium (Fig. 10).

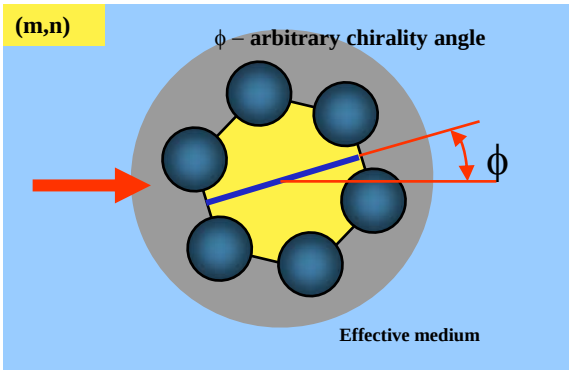

Figure 10. Modeling of chirality effects: carbon ring rotation within CNT

The most problematic regions for simulation are CNT-Me junctions, where atomic structural disorder is observed and the conductivity mechanism is changed. The chirality influence on the resistance in the region of interconnect depends on the number of statistically realized bonds between the CNT

and the catalytic substrate (*e.g.*, Ni, Cu, Au, Ag, Pd, Pt) formed during the CNT growth above the metallic catalyst surface.

4.1. Mechanism of the Ballistic Conductivity as a Result of the Multiple Scattering

We assume that the conducting nanotubes are not very long and electrons are not scattered too much by any defect (imperfection) of this nanomaterial. The effect of the charge accumulation is neglected as well. We are dealing with the so called 'ballistic' mechanism of the electronic transport. This situation is a similar to an ideal billiard with moving elastic balls-electrons. According to the Landauer model [12], $g_{mn} = (e^2/h)\mathbf{Sp}(T_{mn}T_{mn}^{+}), m \neq n$, where g_{mn} are the conductance coefficients while $(e^2/h)T_{12}\Delta\mu$ is the current flow between the two reservoirs with a difference between the chemical potentials $\Delta\mu = \mu_1 - \mu_2$ (T_{12} is the transmission coefficient found to be between 1 to 2 in the one-channel case) based on the conception of the quantum conductance $2e^2/h$ = 0.077 kOhm^{-1} (or, the resistance is about 12.92 kOhm).

Using the simulation models, presented earlier [5], we have developed resistance models for both SW and MW CNT-Me interconnects, based on the interface potential barriers evaluation and Landauer formula, which defines the integrated conductance:

$$G = \frac{2e^2}{h}\sum_{i=1}^{N} T_i = \left(\frac{1}{12.92\,(k\Omega)}\right)\sum_{i=1}^{N} T_i = 0.0774\sum_{i=1}^{N} T_i, \qquad (20)$$

where N is the number of conducting channels and T_i the corresponding transmission coefficient.

4.2. Chirality and Thickness Simulations

On Figure 11 is presented a simulation of catalytic growth of CNT on the metal substrate. This is accompanied by creation of C-Me 'effective bonds'. We should also point out that this is a probabilistic process when only more-or-less equilibrium bonds ("effective bonds") are formed at inter-atomic distances corresponding to the minimum total energies. The evaluation of a number of "effective bonds" using Eq. (20) is principal for the number of "conducting channels", since the conductance is proportional to the number of appeared "effective bonds" within the CNT-Me interconnect.

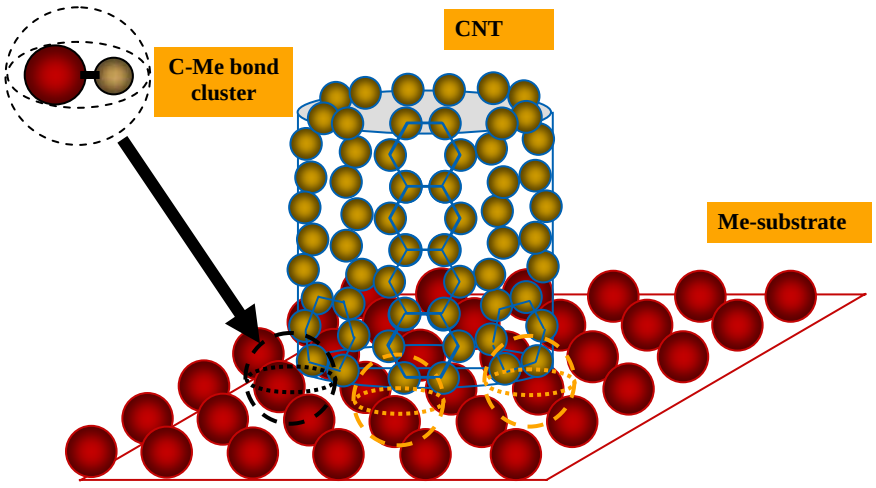

Figure 11. The SW CNT-Me interconnect: model of "*effective bonds*"

The calculation of conducting abilities of "effective bond" leads us to estimate the energy-dependent transparency coefficient of a potential barrier C-Me (Fig. 12), which belongs to scattering problems. The scattering process for a C-Me potential barrier is also regulated by the effect of "thin film" for conductivity electrons, which leads to quantization in voltaic parameters (in the case of full transparency).

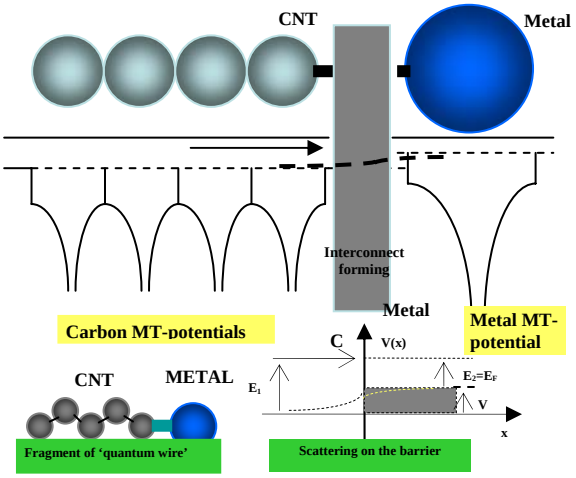

Figure 12. The formation of potential barrier for SW CNT-Me interconnect

The transmission (transparency) coefficient T for the barrier scattering problem (Eq. (20) and Fig. 9) is defined as:

$$T = \sqrt{\frac{E_2}{E_1}}\left(\frac{2\sqrt{E_1}}{\sqrt{E_1}+\sqrt{E_2}}\right)^2, \tag{21}$$

where E_1 and E_2 are the corresponding electron energies.

Evaluation of resistances for CNT-Ni junctions for various nanotube diameters and chiralities are present in Table 1 (see also Figs. 13 and 14). These resistances have been estimated taking into account that only thermally activated electrons (*i.e.*, a small part of all electrons) take a part in the conduction process with Fermi velocity v_F. This ratio can be estimated as:

$$\frac{\Delta \mathrm{n}}{\mathrm{n}} \approx \frac{3}{4}\frac{\mathrm{k}T}{\mathrm{E_F}}, \tag{22}$$

where n is the quasi-free electron concentration, for T = 300^0 K, $\mathrm{k}T = 0.0258$ eV.

Table 1. Simulation of resistances for the SW CNT-Ni interconnects

Diameter, nm	Chirality indices (Fig. 6)	Number of bonds in contact	Modulus of chirality vector, nm	Interconnect resistance, kOhm
zig-zag, $\varphi = 0^\circ$				
1.010	C(13,0)	12	2.952	665,19
2.036	C(26,0)	24	6.394	333,33
5.092	C(65,0)	64	15.990	124,72
10.100	C(130,0)	129	32.002	61,87
20.360	C(260,0)	259	63.940	30,82
armchair, $\varphi = 30^\circ$				
0.949	C(7,7)	12	2.982	665,19
2.035	C(15,15)	28	6.391	205,71
5.021	C(37,37)	72	15.765	111,11
10.041	C(74,74)	146	31.531	54,79
20.084	C(128,128)	294	63.062	27,21
C(3*m*,*m*), $\varphi = 14^\circ$				
0.847	C(9,3)	3	2.66	2666,66
1.694	C(18,6)	5	5.32	1600,00
5.082	C(54,18)	16	15,96	500,00
10.16	C(108,36)	36	32.05	222,22
20.32	C(216,72)	80	64.10	100,00
C(2*m*,*m*), $\varphi = 19^\circ$				
1.036	C(10,5)	5	3.254	1600,00
2.072	C(20,10)	9	6.508	888,88
4.973	C(48,24)	17	15.614	470,50
10.1528	C(98,49)	47	31.880	170,21
20.5128	C(198,99)	97	64.410	82,47

The role of thermally activated electron is described by the scattering mechanism changing in the space of CNT-Me interconnect.The mean free path L in the CNT is of order 10^2–10^4 a_C, where a_C is a carbon covalent radius, which can be explained by the ballistic mechanism of electron transport within the energy channel of the CNT. At the vicinity of interconnect, we observe a drastic decrease of the electron mean free path down to $1 - 2$ a_C. From the uncertainty condition $\kappa L \approx 1$ (where $L \sim a_C \sim 2$ *a.u.* is a free path), we can evaluate the Fermi electron wave number $\kappa \propto \kappa_F \approx 1/a_C \approx 0.5$ a.u.$^{-1}$. It means that $E_F \sim 0.25$ Ry, *i.e.*, a large increase of resistance occurs in the interconnect space. In particular, the variation of the chirality angle ϕ within the interconnect space leads to a fluctuation of the number of C-Me atomic bonds. In the case of $0^o < \phi < 30^o$, a certain number of non-stable and non-equilibrium bonds can be created. Evidently, this leads to a decrease of interconnect conductance, which is well-observed when performing variation of nanotube diameter (Fig. 13):

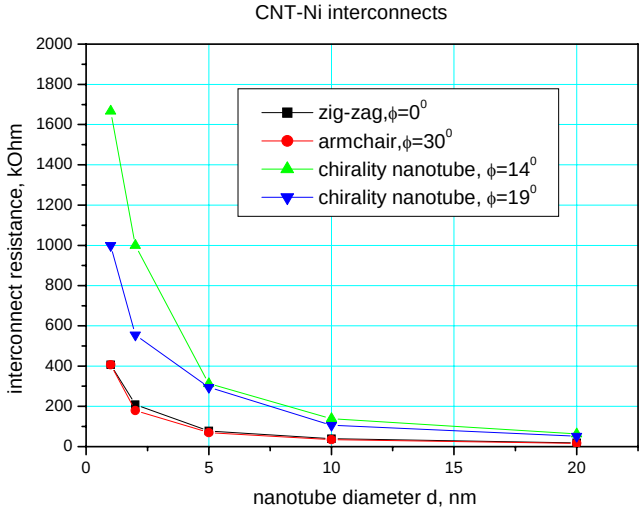

Figure 13. CNT-Ni interconnect resistance *via* NT diameter

Specific results for chirality effect simulations are shown on Figure 14, with an evident maximum of the resistance for $\phi \approx 15^o$, where the large number of non-equilibrium bonds is formed, with higher potential barriers and lower transparency interconnects for the CNT diameter ~1 nm.

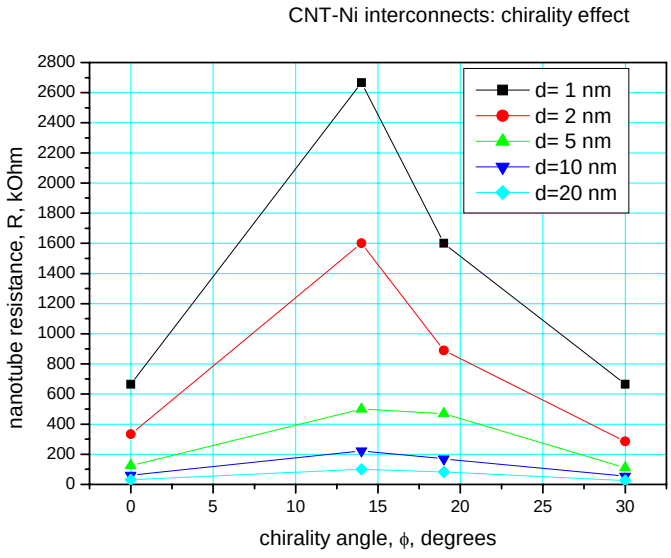

Figure 14. CNT-Ni interconnect simulation: *chirality effects*

On Figure 15 are showed the generalized results of simulations on resistance of junctions obtained for various metallic substrates. It is clear that Ag and Au substrates are more effective electrically while Ni is rather a 'worse' substrate for interconnect, although it yields the most effective catalyst for CNT growth. On the other hand, the catalysts which are usually used for the SW CNT growth (*e.g.*, Fe, Co and Ni), have a stronger bound to the ends of SW CNTs than noble metals [13], *i.e.*, some compromise exists between electrical parameters and strengths of the interconnect bonding.

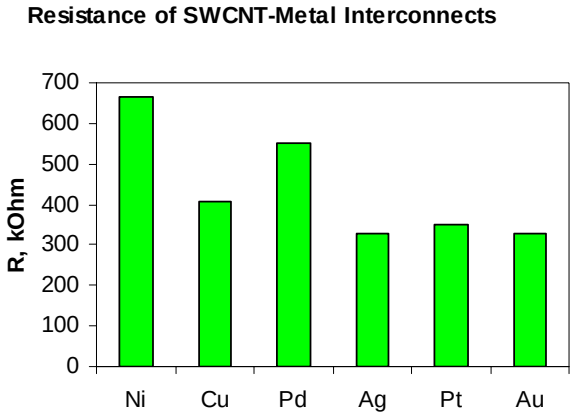

Figure 15. Resistance of the zigzag-type SW CNT-Me

5. Simulations on MW CNT-Me Interconnects: Conductance and Resistance

Our study was focused on the development of models describing the growth mechanism of carbon nanotubes upon nanostructured Ni catalyst inside the pores of Al_2O_3 membranes. The scope of these simulations allows us to predict that a specific morphology of CNTs could be formed inside the specific membranes having defined periodicity and hole dimensions. These simulations are necessary, in order to understand the basic mechanism of CNT growth and to achieve the tight control on the fabrication process. We have constructed atomistic models of both SW CNT bundles and MW CNTs which could fit into a porous alumina with holes diameters ~ 20 – 21 nm. In particular, a multi-shell model of MW CNT is presented on Figure 16, with a pre-defined combination of *armchair* (*ac*) and *zig-zag* (*zz*) shells (Table 2).

Using the simulation models presented earlier [14] we have developed an "effective bonds" model for MWCNT-Me junction resistance, based on the interface potential barriers evaluation and Landauer formula, Eq. (20). Results of these simulations are presented on Figure 17 and in Table 3.

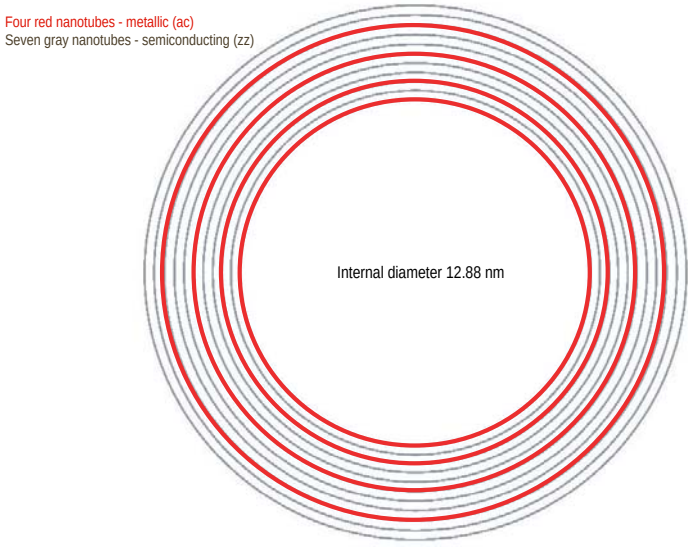

Figure 16. A cross-section of the supercell model for MW CNT with height 6.39 nm and external diameter 19.89 nm

Table 2. Details of the model for MW CNT-Me interconnect

diameter of CNT shell, nm	Chirality
12.88	(95,95) *ac*
13.54	(173,0) *zz*
14.24	(105,105) *ac*
14.87	(190,0) *zz*
15.58	(199,0) *zz*
16.27	(120,120) *ac*
16.99	(217,0) *zz*
17.69	(226,0) *zz*
18.44	(136,136) *ac*
19.18	(245,0) *zz*
19.88	(254,0) *zz*

Again, Figure 17 shows similar ratios of electric resistances as for SW CNTs (Fig. 15), in favour of Au, Ag and Pd. However, in the case of MWCNT-Me junction, the integral mechanical bonding with a corresponding substrate may be not so significant as in the case of SW CNTs, where the weak bonding can be principal.

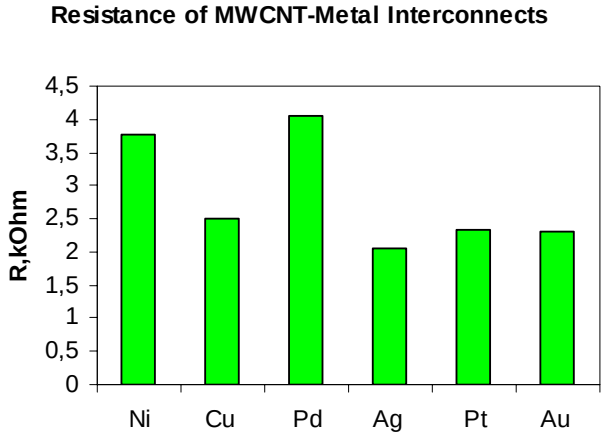

Figure 17. Resistances of various MWCNT- Me interconnects

Table 3. Simulation of resistances for the MW CNT-Me interconnects

Metal	Z	Interconnect resistivity, kOhm
Au	79	2.313
Pt	78	2.345
Pd	47	4.050
Ag	46	2.062
Cu	29	2.509
Ni	28	3.772

6. Evaluation of Current Loss between the Adjacent Shells inside the MW CNT

Using the model of inter-shell potential within the MW CNT we also have evaluated the transparency coefficient, which determines the possible 'radial current' losses. Figure 18 shows the inter-shell potential which is calculated using the developed realistic analytical potentials (see comments of Part 2 and the procedure of the potential construction, *e.g.*, in [2]).

On Figure 18, A is the electron emission energy, E the electron energy, V the height of the potential barrier between the nearest atoms in neighboring nanotube shells. Thus, a radial transparency coefficient T for the two different energy ratios can be defined as:

$$E > V, T = \frac{4Ek_2^2}{(E - k_2^2)\sin^2 k_2 a + 4Ek_2^2}, k_2^2 = E - V, \tag{23}$$

$$E < V, T = \frac{4E\kappa_2^2}{(E - \kappa_2^2)sh^2\kappa_2 a + 4E\kappa_2^2}, \kappa_2^2 = V - E. \quad (24)$$

where k_2 the electron wave number in the case of above-barrier motion and κ_2 the same for under-barrier motion. For example, between the 2nd and 1st shells (*zz-ac* case, Fig. 13) a = 13.54 – 12.88 = 0.66 nm = 12.47 a.u. and $T = 3.469 \cdot 10^{-6}$ *per* 1 bond.

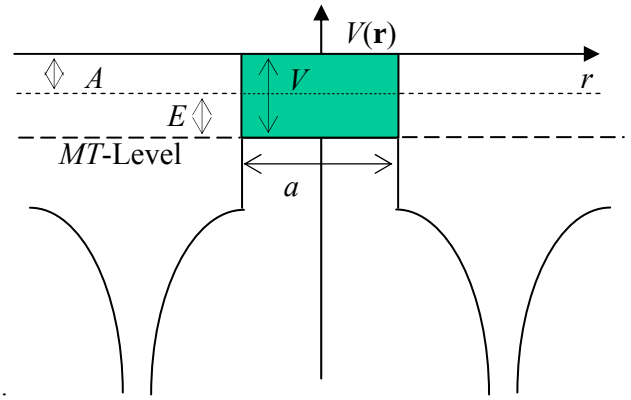

Figure 18. Inter shell transparency and inter-shell *MT*-potential model (*MT*-muffin tin)

Clearly the total radial conductance is proportional to T and the number of effective potential barriers. It is also clear that the 'radial current' losses (or, simply radial current) are similar to the Hall current due to the induced magnetic field of the basic axial current. A pure scattering mechanism is also possible. However, the radial conductance *per* CNT length depends on the morphology (chirality) of the nearest nanotubes, when the number of shortest effective barriers is varied in a probabilistic way. This also means that current-voltage parameters of MW CNTs can be less stable, than in the case of SW CNTs. It was found that inter-shell interactions, such as inter-shell tunneling of electrons and Coulomb interactions [15–17]) cause a reduction of the total MW CNT conductance.

Conclusions

We have predicted the resistance properties of interconnects between the metal substrate (*e.g.*, Ni) and the SW or MW CNTs, using the *'effective bonds'* model. We also expect qualitatively compatible results for the CNT-Me interconnects in both considered approaches, namely, first principles *'liquid metal'* model and empirical *'effective bonds'* model based on the Landauer relationship. The latter is more compatible with experimental measurements, due to the exact description of the local atomic morphology for CNT-Me interconnects.

We have also developed the model of inter-shell interaction in MW CNTs, which allows us to estimate the transparency coefficient as an indicator of possible 'radial current' losses. We point out that a conductance and current-voltage characteristic depends on the morphology of the nearest shell in MWCNT, which means complications for technology and production of nanodevices with stable electric characteristics.

Acknowledgments

This study has been supported by grant EC FP7 ICT-2007-1, Proposal for 21625 CATHERINE Project (2008–2010): *C*arbon n*A*notube *T*echnology for *H*igh-speed n*E*xt-gene*R*ation nano-*I*nterconn*NE*cts. We thank Prof. E. A. Kotomin for stimulating discussions.

References

1. Ahlskog, M., Laurent, Ch., Baxendale, M., Huhtala, M. In: *Encyclopedia of Nanoscience and Nanotechnology / Ed.by H. S. Nalwa*. American Sci. Publishers, 2004. Vol. 3, pp. 139–161.
2. Tans, S. J., Verschueren, R. M., Dekker, C., *Nature,* Vol. 393, 1998, pp. 49–52.

3. Martel, R., Schmidt, T., Shea, H. R., Avouris, Ph., *Appl. Phys. Lett.,* Vol. 73, 1998, pp. 2447–2449.
4. Tersoff, J., *Appl. Phys. Lett***.,** Vol. 74, 1999, pp. 2122–2124.
5. Shunin, Yu. N., Schwartz, K. K. In: *Computer Modelling of Electronic and Atomic Processes in Solids / R. C. Tennyson and A. E. Kiv (Eds.).* Dodrecht / Boston / London: Kluwer Acad. Publishers, 1997, pp. 241–257.
6. Shunin, Yu. N. *Dr. Sc. Habil. Thesis (Phys.&Math.).* Riga-Salaspils, 1991.
7. Economou, E. L. *Green's Functions in Quantum Physics, 3rd edition, Solid State Ser., vol. 7*. Berlin / Heidelberg: Springer Verlag, 2006.
8. Ziman, J. M. *Models of Disorder*. London, New York: Cambridge Univ. Press, 1979.
9. Shunin, Yu. N., Zhukovskii, Yu. F., Bellucci, S., *Computer Modelling & New Technologies,* Vol. 12(2), 2008, pp. 66–77.
10. Smith, N. V., *Phys. Lett. A*, Vol. 26, 1968, pp. 126–127.
11. Soven, P., *Phys. Rev.,* Vol. 156, 1967, pp. 809–813.
12. Stone, D., Szafer, A., *IBM J. Res. Develop*., Vol. 32(3), 1988, pp. 384–413.
13. Ding, F., Larsson, P., Larsson, J. A., Ahuja, R., Duan, H., Rose, A., Bolton, K., *Nano Lett.,* Vol. 8, 2008, pp. 463–468.
14. Shunin, Yu. N. In: *GENNESYS White Paper / H. Dosch and M.H. Van de Voorde (Eds.).* Stuttgart: Max-Planck-Institut für Metallforschung, 2009, pp. 8–29.
15. Uryu, S., *Phys. Rev. B,* Vol. 69, 075402, 2004.
16. Lunde, A. M., Flensberg, K., Jauho, A.-P., *Phys. Rev. B*, Vol. 71, 125408, 2005.
17. Kordrostami, Z., Sheikhi, M. H., Mohammadzadegan, R., *Fullerenes, Nanotubes, and Carbon Nanostructures,* Vol. 16, 2008, pp. 66–77.

Received on the 1st of December, 2009